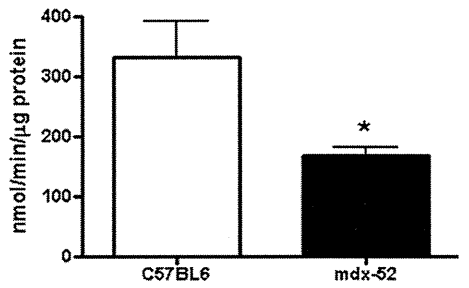

FIG. 6. **Mitochondrial dysfunction in dystrophic muscle.** Gastrocnemius muscle lysates from C57BL/6 and mdx mice (n = 3/group) were analyzed for lactate dehydrogenase activity as an indicator of mitochondrial function in dystrophic and normal muscle. Enzyme activity was assayed biochemically and is represented as the mean ± S.E. (*$p < 0.05$).

efficiency in the liver, muscle, and brain was ≥96% by the F2 generation, which is in agreement with earlier reports (18, 22, 23).

Comparison of the proteomes of skeletal muscle of the mdx and control mice using the differential SILAC strategy identified previously known, as well as novel, pathways associated with dystrophin deficiency. Approximately 750 to 850 proteins were identified and quantified in the gastrocnemius muscle. These numbers are similar to those previously reported in other skeletal muscle proteome studies (29, 30). However, these numbers are lower than those from a recent study in which a highly sensitive mass spectrometer was used on samples that were subjected to extensive fractionation (31). The identification of a low number of proteins in skeletal muscle can be attributed to the huge dynamic range between high and low abundant proteins in the skeletal muscle tissue (32). Indeed, skeletal muscle is mainly composed of structural proteins such as myosin and actin, which account for more than 40% of the total proteins and thus mask the detection of low-abundant proteins.

Initial SILAC proteome profiling was performed on pairs of labeled-normal and unlabeled-normal mice and of labeled-normal and unlabeled-mdx mice. As expected, we observed a complete absence of dystrophin expression and the down-regulation of dystroglycan complex in the mdx muscle. Furthermore, greater differential protein expression was observed when comparing dystrophin-deficient to normal gastrocnemius muscle, whereas only a few proteins were altered between labeled and unlabeled normal gastrocnemius muscle. To statistically validate the initial findings, we performed spike-in SILAC using an independent set of normal and mdx mice. Of the total number of proteins identified and quantified, ~73 were found to be significantly altered in their levels between dystrophin-deficient and normal ($p < 0.05$) mice. The top candidate proteins included vimentin, desmin, annexin-II, ribosomal proteins, GRP78, and actinins whose levels were increased in dystrophin-deficient muscle. The enhanced expression of these proteins in dystrophic muscle indicates the perturbation of various signaling mechanisms. The high levels of vimentin and other extracellular matrix proteins were maintained in the diaphragm of a 22-month-old mdx mouse (33). These data suggest that vimentin is increased very early and stays up-regulated during disease progression. In addition, our results indicate a significant up-regulation of GRP78 (a stress-related protein; chaperone) in dystrophic muscle, suggesting the activation of stress responses early in the disease process. Our profiling results also identified significant down-regulation of the contractile apparatus (*e.g.* myosin and tropomyosin) and significant down-regulation of proteins involved in mitochondrial energy metabolism such as L-lactate dehydrogenase B chain, 3,2-trans-enoyl-CoA isomerase, and trifunctional enzyme subunit alpha. These results might suggest that the perturbed mitochondrial energy metabolism and the underlying muscle weakness occur very early in the pathogenesis of dystrophin deficiency.

Some earlier studies examined protein changes in dystrophic hind limb muscles, diaphragm, heart, and extraocular muscles of mdx mice at different ages; however, few studies involved dystrophic gastrocnemius muscle (9–12, 34–37). A study using a 2-DE approach reported a 4-fold decrease in adenylate kinase levels in the hind limb muscles of 3-month-old mdx mice relative to C57BL/10 muscles (9). Our proteomic analyses identified adenylate kinase in the gastrocnemius muscle (with at least 12 peptides and 50% sequence coverage); however, no significant difference was observed in the relative abundance of adenylate kinase between mdx and C57BL/6. The disparity in the proteomic alterations observed between these studies can be attributed to the differences in the strain, age, and type of muscles tested. Doran *et al.* conducted a series of proteomic profiling studies in dystrophin-deficient skeletal muscle and diaphragm (10, 11) and reported a significant decrease in calsequestrin levels in the skeletal muscle of 9-week-old mdx mice relative to controls (11). Those authors also reported the reduced expression of regucalcin and sarcalumenin (an intracellular Ca^{+2} signaling protein) in both young and aged mdx diaphragm, indicating abnormal cytosolic calcium handling in dystrophin-deficient muscle. Even though our proteomic analyses identified calsequestrin (with at least 10 peptides and 20% sequence coverage), no significant difference was observed in its relative abundance between mdx and C57BL/6. We did not detect regucalcin, but we did detect sarcalumenin with good peptide numbers and sequence coverage; however, no significant alteration was noted in the relative abundance of these proteins. The current study used isolated gastrocnemius muscle from perfused mice for the analyses, whereas other studies used either diaphragm or hind limb muscles (a mixture of several muscle groups). It is unclear whether the tissues in other studies were collected from perfused or non-perfused mice. The differences in the tissues and techniques used might be responsible for the discrepant results of these studies. Another study reported an increase in cardiovascular heat

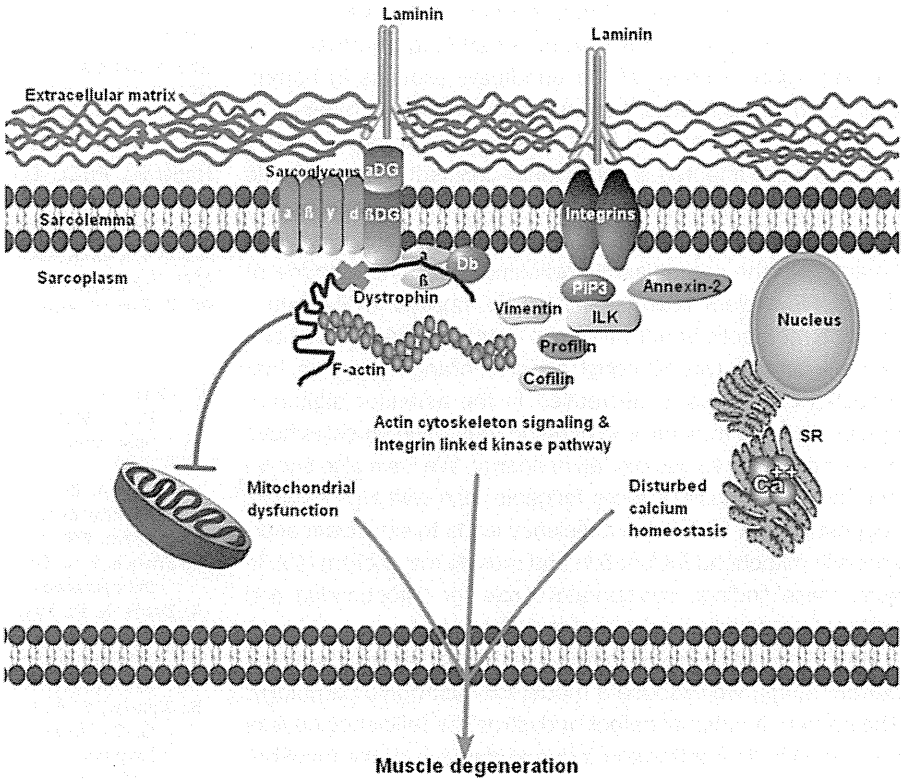

FIG. 7. **Pathways involved in the pathogenesis of dystrophic muscle.** An absence of dystrophin leads to the compensatory up-regulation of actin cytoskeletal signaling and ILK pathway activation to reduce contraction-induced injury in skeletal muscle. In parallel, reduced mitochondrial function, along with disturbances in calcium homeostasis, exacerbate the disease phenotype.

shock protein in dystrophin-deficient diaphragm (12). Our proteomic profiling did not identify cardiovascular heat shock protein, but several other heat shock proteins were identified. We did not observe significant differences in heat shock proteins between mdx and C57BL/6. However, additional comparative evaluations are needed in order to sort out whether these differences between studies are technical or biological in nature.

IPA was used to delineate the perturbed molecular networks associated with altered protein levels. The significantly altered canonical networks included actin cytoskeleton signaling, ILK pathways, glycolysis, the citrate cycle, and mitochondrial function. These results indicate the usefulness of the current method for identifying multiple perturbed pathways in a single analysis, and suggest that it might be useful for understanding disease processes at the systems level. The validation of data by means of immunoblotting and the complete agreement of these results with the proteomic profiling results indicate the robustness of the SILAC mouse strategy. Furthermore, the utilization of biochemical assays also validated the presence of perturbed mitochondrial function, although no changes in protein levels were detected via immunoblotting in the dystrophic muscle. This suggests that subtle differences can also be measured using the SILAC mouse strategy.

The identification of the involvement of the actin cytoskeletal signaling and ILK pathways in dystrophic pathology early in the disease process is an important finding. Indeed, the silencing of ILK expression in skeletal muscles of mice using a cre/lox system has shown the role of the ILK pathway in causing muscle pathology (38). The deletion of ILK led to the development of progressive muscular dystrophy, which was accompanied by degenerating myofibers and fibrosis, and these features were more severe near the myofascial junctions (39). A subsequent report also showed that skeletal muscle expresses high levels of ILK, predominantly at myotendinous junctions and costameres. Further, it was reported that ILK binds the cytoplasmic domain of beta-1 integrin and mediates the phosphorylation of protein kinase B/Akt, which in turn plays a central role during skeletal muscle regeneration. In addition, an association between beta-1 integrin and insulin-like growth factor 1 receptor was also shown in muscle, and this association is considered critical for insulin-like growth factor 1 receptor/insulin receptor substrate signaling to protein kinase B/Akt during mechanical stress in skeletal muscle (38). Taken together, these results indicate that the up-regulation of the ILK and actin cytoskeletal pathways might be a compensatory mechanism to overcome the loss of dystrophin protein and help protect the susceptible myofiber membrane from contraction-induced damage.

The exploitation of integrin-signaling and related pathways as therapeutic targets for DMD appears promising, as the enhanced expression of beta-1D integrin in dystrophic muscle decreases the damaged myofibers and is attributed to the presence of more functional integrin at the sarcolemma (40). The modulation of these pathways in dystrophic mdx muscle

via chemical mediators or drugs should provide valuable insight into their specific role in muscle pathology. Furthermore, the validation of some of the candidate proteins in human DMD samples suggests their relevance to human disease.

Our study showed that the levels of several mitochondrial proteins were affected in dystrophin-deficient muscle. A role for mitochondria in dystrophic pathology has been observed previously (41–44). An increase in Ca^{2+}content has been detected in the sarcoplasmic reticulum and mitochondria of dystrophic skeletal muscle, along with impaired ATP production and metabolic abnormalities (41–44). In addition, we have recently shown (via 10-nonyl acridine orange staining) that mitochondrial mass is decreased in the extensor digitorum longus fibers of mdx mice, indicating that these muscles have a lower capacity to use oxidative energy. We have also shown that the mdx muscle is more fatigable than wild-type muscle, suggesting that dystrophin deficiency leads to significant alterations in mitochondrial function and muscle metabolism (45). In sum, these findings corroborate a role for mitochondria and metabolic pathways in dystrophic pathology.

Based on previously published data and the results of our current study, we propose a model for dystrophic pathology. The primary functional defect of dystrophin deficiency causes susceptibility to contraction-induced damage of the myofiber membranes. The injured fibers cause the compensatory upregulation of actin cytoskeletal and ILK pathways in order to protect from further damage. In parallel, dystrophin-deficient myofiber might have leaky Ca^{2+} channels, which would enhance the Ca^{2+} influx into dystrophic fibers, leading to protease activation and free radical formation from cytosolic and mitochondrial sources; this would cause the dysregulation of mitochondria, energy metabolism, and calcium homeostasis. The activation of these pathways can potentially lead to myofiber damage and progression of the dystrophic pathology (Fig. 7). Based on this model, we can speculate that therapies that simultaneously target multiple perturbed pathways might be beneficial for DMD patients and have the potential to ameliorate dystrophic pathology.

Acknowledgments—Sree Rayavarapu is a pre-doctoral candidate in the Molecular Medicine Program of the Institute for Biomedical Sciences at the George Washington University; this work is from a dissertation to be presented to this program in partial fulfillment of the requirements for a Ph.D. degree. The authors thank Drs. Susan Knoblach and Terrence Partridge for their technical help and advice regarding this work. The authors also thank Dr. Deborah McClellan for editing this manuscript.

* Sree Rayavarapu is supported by a pre-doctoral fellowship from Association Francaise Contreles Myopathies. This work was partially supported by National Institute of Health (NIAMS) 5P50AR060836-02 and by NIH core grants NCMRR/NINDS 2R24HD050846-06 (National Center for Medical Rehabilitation Research), IDDRC 5P30HD040677-10 (Intellectual and Developmental Disabilities Research Center), and NIH NCRR UL1RR031988 (GWU-CNMC CTSI). This work is also supported by following NIH (RO1 AR050478, ARO55686; K26OD011171; 1U54HD071601; 2R24HD050846-06) and DOD grants (W81XWH-11-1-0330; W81XWH-11-1-0782; W81XWH-10-1-0659; W81XWH-11-1-0809; W81XWH-09-1-0599) and a translational research grant from MDA and pilot grant from PPMD.

[S] This article contains supplemental material.

‖ To whom correspondence should be addressed: Kanneboyina Nagaraju, Ph.D., D.V.M., Professor of Integrative Systems Biology and Pediatrics, the George Washington University; Director, Murine Drug Testing Facility; Associate Director, Research Center for Genetic Medicine, Children's National Medical Center, 111 Michigan Avenue NW, Washington, D.C. 20010. Tel.: (202) 476-6220; Fax: (202) 476-6014; E-mail: knagaraju@cnmcresearch.org.

REFERENCES

1. Petrof, B. J., Shrager, J. B., Stedman, H. H., Kelly, A. M., and Sweeney, H. L. (1993) Dystrophin protects the sarcolemma from stresses developed during muscle contraction. *Proc. Natl. Acad. Sci. U.S.A.* **90,** 3710–3714
2. Oak, S. A., Zhou, Y. W., and Jarrett, H. W. (2003) Skeletal muscle signaling pathway through the dystrophin glycoprotein complex and Rac1. *J. Biol. Chem.* **278,** 39287–39295
3. Spence, H. J., Chen, Y. J., and Winder, S. J. (2002) Muscular dystrophies, the cytoskeleton and cell adhesion. *Bioessays* **24,** 542–552
4. Evans, N. P., Misyak, S. A., Robertson, J. L., Bassaganya-Riera, J., and Grange, R. W. (2009) Dysregulated intracellular signaling and inflammatory gene expression during initial disease onset in Duchenne muscular dystrophy. *Am. J. Phys. Med. Rehabil.* **88,** 502–522
5. Spurney, C. F., Gordish-Dressman, H., Guerron, A. D., Sali, A., Pandey, G. S., Rawat, R., Van Der Meulen, J. H., Cha, H. J., Pistilli, E. E., Partridge, T. A., Hoffman, E. P., and Nagaraju, K. (2009) Preclinical drug trials in the mdx mouse: assessment of reliable and sensitive outcome measures. *Muscle Nerve* **39,** 591–602
6. Sicinski, P., Geng, Y., Ryder-Cook, A. S., Barnard, E. A., Darlison, M. G., and Barnard, P. J. (1989) The molecular basis of muscular dystrophy in the mdx mouse: a point mutation. *Science* **244,** 1578–1580
7. Araki, E., Nakamura, K., Nakao, K., Kameya, S., Kobayashi, O., Nonaka, I., Kobayashi, T., and Katsuki, M. (1997) Targeted disruption of exon 52 in the mouse dystrophin gene induced muscle degeneration similar to that observed in Duchenne muscular dystrophy. *Biochem. Biophys. Res. Commun.* **238,** 492–497
8. Collins, C. A., and Morgan, J. E. (2003) Duchenne's muscular dystrophy: animal models used to investigate pathogenesis and develop therapeutic strategies. *Int. J. Exp. Pathol.* **84,** 165–172
9. Ge, Y., Molloy, M. P., Chamberlain, J. S., and Andrews, P. C. (2003) Proteomic analysis of mdx skeletal muscle: great reduction of adenylate kinase 1 expression and enzymatic activity. *Proteomics* **3,** 1895–1903
10. Doran, P., Dowling, P., Donoghue, P., Buffini, M., and Ohlendieck, K. (2006) Reduced expression of regucalcin in young and aged mdx diaphragm indicates abnormal cytosolic calcium handling in dystrophin-deficient muscle. *Biochim. Biophys. Acta* **1764,** 773–785
11. Doran, P., Dowling, P., Lohan, J., McDonnell, K., Poetsch, S., and Ohlendieck, K. (2004) Subproteomics analysis of Ca+-binding proteins demonstrates decreased calsequestrin expression in dystrophic mouse skeletal muscle. *Eur. J. Biochem.* **271,** 3943–3952
12. Doran, P., Martin, G., Dowling, P., Jockusch, H., and Ohlendieck, K. (2006) Proteome analysis of the dystrophin-deficient MDX diaphragm reveals a drastic increase in the heat shock protein cvHSP. *Proteomics* **6,** 4610–4621
13. Ong, S. E., Blagoev, B., Kratchmarova, I., Kristensen, D. B., Steen, H., Pandey, A., and Mann, M. (2002) Stable isotope labeling by amino acids in cell culture, SILAC, as a simple and accurate approach to expression proteomics. *Mol. Cell. Proteomics* **1,** 376–386
14. Emadali, A., and Gallagher-Gambarelli, M. (2009) [Quantitative proteomics by SILAC: practicalities and perspectives for an evolving approach]. *Med. Sci. (Paris)* **25,** 835–842
15. Blagoev, B., Kratchmarova, I., Ong, S. E., Nielsen, M., Foster, L. J., and Mann, M. (2003) A proteomics strategy to elucidate functional protein-protein interactions applied to EGF signaling. *Nat. Biotechnol.* **21,** 315–318
16. Kruger, M., Kratchmarova, I., Blagoev, B., Tseng, Y. H., Kahn, C. R., and

Mann, M. (2008) Dissection of the insulin signaling pathway via quantitative phosphoproteomics. *Proc. Natl. Acad. Sci. U.S.A.* **105,** 2451–2456
17. Amanchy, R., Kalume, D. E., Iwahori, A., Zhong, J., and Pandey, A. (2005) Phosphoproteome analysis of HeLa cells using stable isotope labeling with amino acids in cell culture (SILAC). *J. Proteome Res.* **4,** 1661–1671
18. Kruger, M., Moser, M., Ussar, S., Thievessen, I., Luber, C. A., Forner, F., Schmidt, S., Zanivan, S., Fassler, R., and Mann, M. (2008) SILAC mouse for quantitative proteomics uncovers kindlin-3 as an essential factor for red blood cell function. *Cell* **134,** 353–364
19. McClatchy, D. B., Liao, L., Park, S. K., Xu, T., Lu, B., and Yates, J. R., III (2011) Differential proteomic analysis of mammalian tissues using SILAM. *PLoS One* **6,** e16039
20. McClatchy, D. B., and Yates, J. R., 3rd (2008). Stable isotope labeling of mammals (SILAM). *CSH Protoc.* **2008,** pdb.prot4940
21. Lu, X. M., Tompkins, R. G., and Fischman, A. J. (2012) SILAM for quantitative proteomics of liver Akt1/PKBalpha after burn injury. *Int. J. Mol. Med.* **29,** 461–471
22. Huang, T. C., Sahasrabuddhe, N. A., Kim, M. S., Getnet, D., Yang, Y., Peterson, J. M., Ghosh, B., Chaerkady, R., Leach, S. D., Marchionni, L., Wong, G. W., and Pandey, A. (2012) Regulation of lipid metabolism by dicer revealed through SILAC mice. *J. Proteome Res.* **11,** 2193–2205
23. Zanivan, S., Krueger, M., and Mann, M. (2012) In vivo quantitative proteomics: the SILAC mouse. *Methods Mol. Biol.* **757,** 435–450
24. Monetti, M., Nagaraj, N., Sharma, K., and Mann, M. (2011) Large-scale phosphosite quantification in tissues by a spike-in SILAC method. *Nat. Methods* **8,** 655–658
25. Geiger, T., Wisniewski, J. R., Cox, J., Zanivan, S., Kruger, M., Ishihama, Y., and Mann, M. (2011) Use of stable isotope labeling by amino acids in cell culture as a spike-in standard in quantitative proteomics. *Nat. Protoc.* **6,** 147–157
26. Jahnke, V. E., Sabido, O., Defour, A., Castells, J., Lefai, E., Roussel, D., and Freyssenet, D. (2010) Evidence for mitochondrial respiratory deficiency in rat rhabdomyosarcoma cells. *PLoS One* **5,** e8637
27. Larance, M., Bailly, A. P., Pourkarimi, E., Hay, R. T., Buchanan, G., Coulthurst, S., Xirodimas, D. P., Gartner, A., and Lamond, A. I. (2011) Stable-isotope labeling with amino acids in nematodes. *Nat. Methods.* **8,** 849–851
28. Sury, M. D., Chen, J. X., and Selbach, M. (2010) The SILAC fly allows for accurate protein quantification in vivo. *Mol. Cell. Proteomics* **9,** 2173–2183
29. Hojlund, K., Yi, Z., Hwang, H., Bowen, B., Lefort, N., Flynn, C. R., Langlais, P., Weintraub, S. T., and Mandarino, L. J. (2008) Characterization of the human skeletal muscle proteome by one-dimensional gel electrophoresis and HPLC-ESI-MS/MS. *Mol. Cell. Proteomics* **7,** 257–267
30. Gelfi, C., Vasso, M., and Cerretelli, P. (2011) Diversity of human skeletal muscle in health and disease: contribution of proteomics. *J. Proteomics* **74,** 774–795
31. Drexler, H. C., Ruhs, A., Konzer, A., Mendler, L., Bruckskotten, M., Looso, M., Gunther, S., Boettger, T., Kruger, M., and Braun, T. (2012). On marathons and sprints: an integrated quantitative proteomics and transcriptomics analysis of differences between slow and fast muscle fibers. *Mol. Cell. Proteomics* **11,** M111.010801
32. Ohlendieck, K. (2011) Skeletal muscle proteomics: current approaches, technical challenges and emerging techniques. *Skelet. Muscle* **1,** 6
33. Carberry, S., Zweyer, M., Swandulla, D., and Ohlendieck, K. (2012) Proteomics reveals drastic increase of extracellular matrix proteins collagen and dermatopontin in the aged mdx diaphragm model of Duchenne muscular dystrophy. *Int. J. Mol. Med.* **30,** 229–234
34. Doran, P., Wilton, S. D., Fletcher, S., and Ohlendieck, K. (2009) Proteomic profiling of antisense-induced exon skipping reveals reversal of pathobiochemical abnormalities in dystrophic mdx diaphragm. *Proteomics* **9,** 671–685
35. Lewis, C., Doran, P., and Ohlendieck, K. (2012) Proteomic analysis of dystrophic muscle. *Methods Mol. Biol.* **798,** 357–369
36. Lewis, C., and Ohlendieck, K. (2010) Proteomic profiling of naturally protected extraocular muscles from the dystrophin-deficient mdx mouse. *Biochem. Biophys. Res. Commun.* **396,** 1024–1029
37. Alagaratnam, S., Mertens, B. J., Dalebout, J. C., Deelder, A. M., van Ommen, G. J., den Dunnen, J. T., and Hoen, P. A. (2008). Serum protein profiling in mice: identification of Factor XIIIa as a potential biomarker for muscular dystrophy. *Proteomics* **8,** 1552–1563
38. Wang, H. V., Chang, L. W., Brixius, K., Wickstrom, S. A., Montanez, E., Thievessen, I., Schwander, M., Muller, U., Bloch, W., Mayer, U., and Fassler, R. (2008) Integrin-linked kinase stabilizes myotendinous junctions and protects muscle from stress-induced damage. *J. Cell Biol.* **180,** 1037–1049
39. Gheyara, A. L., Vallejo-Illarramendi, A., Zang, K., Mei, L., St-Arnaud, R., Dedhar, S., and Reichardt, L. F. (2007) Deletion of integrin-linked kinase from skeletal muscles of mice resembles muscular dystrophy due to alpha 7 beta 1-integrin deficiency. *Am. J. Pathol.* **171,** 1966–1977
40. Liu, J., Milner, D. J., Boppart, M. D., Ross, R. S., and Kaufman, S.J. (2012) beta1D chain increases alpha7beta1 integrin and laminin and protects against sarcolemmal damage in mdx mice. *Hum. Mol. Genet.* **21,** 1592–1603
41. Robert, V., Massimino, M. L., Tosello, V., Marsault, R., Cantini, M., Sorrentino, V., and Pozzan, T. (2001) Alteration in calcium handling at the subcellular level in mdx myotubes. *J. Biol. Chem.* **276,** 4647–4651
42. Lucas-Heron, B., Schmitt, N., and Ollivier, B. (1990) Muscular dystrophy: possible role of mitochondrial deficiency in muscle degeneration processes. *J. Neurol. Sci.* **95,** 327–334
43. Hopf, F. W., Turner, P. R., and Steinhardt, R. A. (2007) Calcium misregulation and the pathogenesis of muscular dystrophy. *Subcell. Biochem.* **45,** 429–464
44. Whitehead, N. P., Yeung, E. W., and Allen, D. G. (2006) Muscle damage in mdx (dystrophic) mice: role of calcium and reactive oxygen species. *Clin. Exp. Pharmacol. Physiol.* **33,** 657–662
45. Jahnke, V. E., Van Der Meulen, J. H., Johnston, H. K., Ghimbovschi, S., Partridge, T., Hoffman, E. P., and Nagaraju, K. (2012) Metabolic remodeling agents show beneficial effects in the dystrophin-deficient mdx mouse model. *Skelet. Muscle* **2,** 16

SCIENTIFIC REPORTS

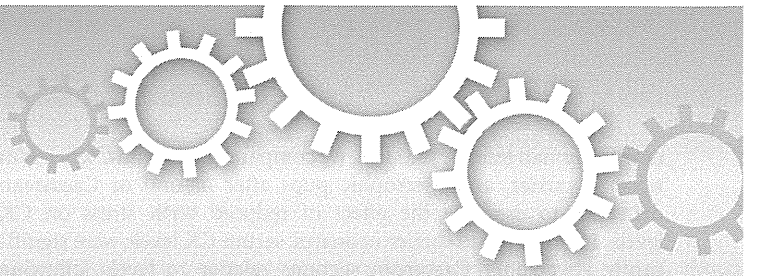

OPEN

SUBJECT AREAS:
DISEASE MODEL
NEUROMUSCULAR DISEASE
TRANSCRIPTIONAL REGULATORY ELEMENTS
MOLECULAR NEUROSCIENCE

Received
17 April 2013

Accepted
25 June 2013

Published
15 July 2013

Correspondence and requests for materials should be addressed to S.T. (takeda@ncnp.go.jp)

Initial Pulmonary Respiration Causes Massive Diaphragm Damage and Hyper-CKemia in Duchenne Muscular Dystrophy Dog

Akinori Nakamura[1,2], Masanori Kobayashi[1,3], Mutsuki Kuraoka[1], Katsutoshi Yuasa[1], Naoko Yugeta[4], Takashi Okada[1] & Shin'ichi Takeda[1]

[1]Department of Molecular Therapy, National Institute of Neuroscience, National Center of Neurology and Psychiatry, 4-1-1 Ogawa-higashi, Kodaira, Tokyo 187-8502, Japan, [2]Department of Medicine (Neurology and Rheumatology), Shinshu University School of Medicine, 3-1-1 Asahi, Matsumoto 390-8621, Japan, [3]Department of Reproduction, Nippon Veterinary and Life Science University (NVLU) 1-7-1, Kyonan-cho, Musashino, Tokyo, 180-8602, Japan, [4]Department of Surgery I, Azabu University, 1-17-71 Fuchinobe, Sagamihara, 229-8501, Japan.

The molecular mechanism of muscle degeneration in a lethal muscle disorder Duchene muscular dystrophy (DMD) has not been fully elucidated. The dystrophic dog, a model of DMD, shows a high mortality rate with a marked increase in serum creatine kinase (CK) levels in the neonatal period. By measuring serum CK levels in cord and venous blood, we found initial pulmonary respiration resulted in massive diaphragm damage in the neonates and thereby lead to the high serum CK levels. Furthermore, molecular biological techniques revealed that osteopontin was prominently upregulated in the dystrophic diaphragm prior to the respiration, and that immediate-early genes (*c-fos* and *egr-1*) and inflammation/immune response genes (IL-6, IL-8, COX-2, and selectin E) were distinctly overexpressed after the damage by the respiration. Hence, we segregated dystrophic phases at the molecular level before and after mechanical damage. These molecules could be biomarkers of muscle damage and potential targets in pharmaceutical therapies.

Duchenne muscular dystrophy (DMD) is characterized by a progressive muscular atrophy and weakness resulting from a mutation in the *DMD* gene, which encodes the structural protein dystrophin. Dystrophin maintains the stability of the cell membrane of the muscle fibers, during muscle contraction and relaxation and regulates intracellular calcium homeostasis[1]. Dystrophin-deficient muscles are thought to be vulnerable during muscle contraction, and resultant breaks in the sarcolemma increase the intracellular free calcium concentration and thereby trigger calcium-activated proteases and fiber necrosis[2]. However, the precise molecular mechanism of muscle degeneration in dystrophic muscle has not been fully elucidated since muscle regeneration is very active in the conventional *mdx* mouse model[3]. For the development of a pathology-based therapy and the prevention of disease progression, a better understanding of dystrophic pathology is needed.

The dystrophic dog, one of the animal models of DMD, shows a high mortality rate with a prominent increase in serum level of creatine kinase (CK) in the neonatal period[4,5]. This is of interest because DMD human newborns also show high serum or plasma CK levels[6–8], but the molecular nature of increase in the CK levels in newborns has not yet been fully elucidated. Because of this similarity in CK levels, our research has focused on understanding the molecular mechanism underlying this distinct event in neonatal dystrophic dogs.

Here, we for the first time presented that the initial respiration causes massive diaphragm damage and that osteopontin was prominently upregulated in the dystrophic diaphragm prior to the initial respiration and that the immediate-early genes *c-fos* and *egr-1* and interleukin-6 and -8 were immediately overexpressed after the damage from the initial respiration. Our results segregate dystrophic phases at the molecular level before and after mechanical damage, and the gene and molecules may not only be new biomarkers of muscle damage, but also molecular targets of pharmaceutical therapies.

Results

Initial pulmonary respiration caused diaphragm damage in neonatal dystrophic dogs. Physical stresses (e.g., compression in the birth canal) have been postulated to be causative factors of the increased serum CK levels in

normal human infants[8–10]. Thus, we compared the serum CK levels in normal, carrier, and dystrophic pups after natural or Caesarean deliveries to examine the effect of reduced birth stress on CK levels. In normal and carrier neonates, serum CK levels were significantly lower after Caesarean sections relative to levels following natural delivery, while no difference was observed for dystrophic neonates (Figure 1A). These observations suggest that the stress of natural delivery is not a major causative factor in the increased CK levels of dystrophic dog neonates.

To determine whether the cause of neonatal increased CK levels could be related to initial pulmonary respiration, we obtained blood from the umbilical cords after the Caesarean sections, which reflect the condition before the initial respiration, and blood from the jugular vein 1 hour after initial respiration to compare the serum CK levels among the different groups of dogs. No differences in the serum CK levels were observed between the venous blood and cord blood of normal and carrier dogs (Figure 1B). However, the CK levels were 5 times higher in the cord blood of the dystrophic dogs than in that of the normal dogs and 35 times higher in the dystrophic venous blood than in the dystrophic cord blood. Serum CK values had increased rapidly 30 min after the initial respiration and peaked between 4 and 8 hours after it (Figure 1C). The histopathology of the dystrophic diaphragm before respiration revealed a slight increase in the number of calcium-positive opaque fibers, which showed a slight infiltration of CD18-positive neutrophils, but cleaved caspase 3-positive apoptotic fibers were not observed (Figure 1D and Supplementary Figure 1). Further, we found larger interstitial spaces, massive opaque fibers indicating hyaline degeneration, and a slight increase in neutrophils after the beginning of respiration, but caspase-3 apoptotic-positive fibers, C5b-9-positive necrotic fibers and LC3-positive autophagic fibers were not overt (Supplementary Figure 1).

Tibialis cranialis (TC) muscle in dystrophic dogs before and after the respiration showed some opaque fibers, but no hyaline degeneration likely to diaphragm (Supplementary Figure 2). Whilst heart (left ventricle) muscle in dystrophic dogs both before and after the respiration did not present any pathological changes. Thus, we have considered that the dramatic increase in serum CK levels after the respiration is due to the specific damage of diaphragm, but not of skeletal or heart muscle. We also have examined the histopathology of 1, 2, and 3 weeks post-natal diaphragm. Serum CK levels have been drastically decreased in these dystrophic dogs and the histopathology of dystrophic diaphragm at 1 week of age was less severe compared to that at birth. Each histopathology at 2 or 3 weeks of age was not much different from at 1 week of age (Supplementary Figure 3). We, however, could not declare these findings are definitely due to a

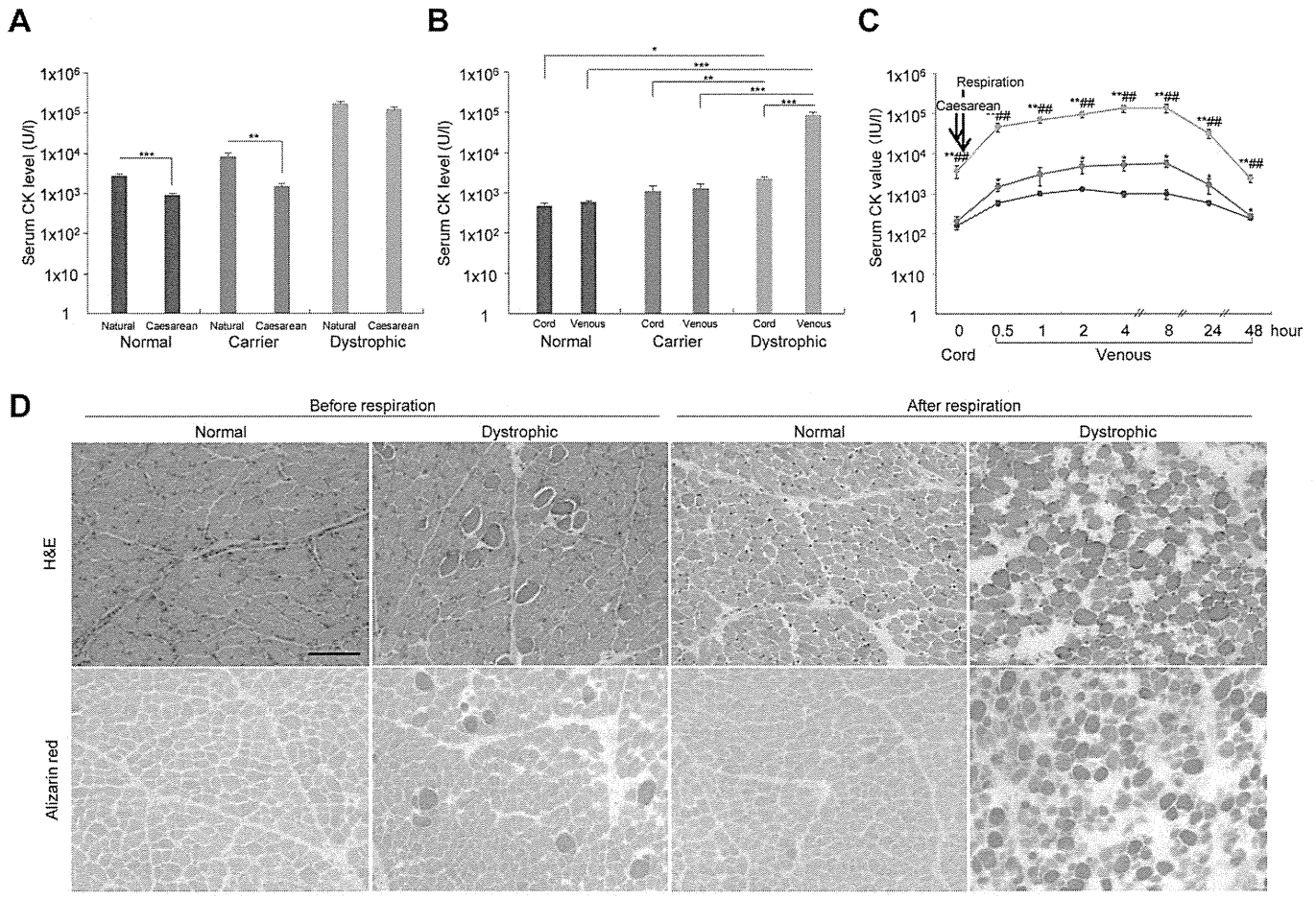

Figure 1 | A marked increase in serum creatine (CK) levels and hyaline degeneration in the diaphragm of neonatal dystrophic dogs after initial pulmonary respiration. (A) The serum CK levels in neonatal normal (n = 71), carrier (n = 37), and dystrophic (n = 41) dogs were compared after natural and elective Cesarean deliveries. ** $p < 0.01$; *** $p < 0.001$. (B) Serum CK levels in the cord and venous blood after initial respiration in normal (n = 5), carrier (n = 3), and dystrophic (n = 6) dogs. * $p < 0.05$; ** $p < 0.01$; *** $p < 0.001$. (C) Time course of changes in serum CK levels in cord and venous blood after initial respiration in normal (black; n = 5), carrier (red; n = 3), and dystrophic (blue; n = 6) dogs. * $p < 0.05$ dystrophic *vs.* normal, ** $p < 0.01$ dystrophic *vs.* normal or dystrophic *vs.* carrier; ## $p < 0.01$: dystrophic *vs.* carrier. (D) Hematoxylin-eosin (H&E) and alizarin red staining of diaphragms of normal and dystrophic dogs before respiration and 1 hour after respiration. Muscle stained by alizarin red indicates a high cytosolic calcium concentration. Bar indicates 100 μm.

remakable capacity to self-recover, since the phenotypic severity is different among the dogs[5]. Moreover, we noticed the degeneration of affected diaphragm was not diffuse and resulted in white streaks[5]. Number of examined affected dogs is limited at early period after birth. Therefore, we concluded that the findings of 1, 2, and 3 weeks post-natal diaphragm suggested recovery of diaphragm at certain extents, which was also indicated by the change of serum CK levels after birth.

Differentially upregulated genes in dystrophic diaphragm before and after initial respiration. Next, we carried out cDNA microarray experiments to determine the genes differentially upregulated genes before and after initial respiration in the dystrophic diaphragm, to identify genes and molecules participating in the dystrophic pathology. Many more genes were differentially upregulated (> 3-fold change) in the dystrophic diaphragm compared to normal before and after initial respiration (Figure 2A and B, respectively). In the comparison, the increase in number of upregulated genes was related to membrane and inflammation/immune response before the respiration (Table 1 and Supplementary Table 1), and to the membrane and transcription/signal transduction after the respiration (Table 2 and Supplementary Table 1). After the respiration compared to before, the pattern of differentially upregulated genes were generally consistent between dystrophic and normal diaphragm (Table 3, 4, and Supplementary Table 1); however, some particular transcription/signal transduction and inflammation/immune response genes were distinctly increased in dystrophic diaphragm (Figure 2B, 2D, and Supplementary Table 1).

Upregulated genes in the dystrophic dog diaphragm before the initial respiration. We selected genes on the microarrays that were increased over 10-fold change before and after the initial respiration in the dystrophic diaphragm relative to the normal (Figure 2 and Supplementary Table 1). Prior to the initial respiration, osteopontin mRNA was most prominently upregulated in the dystrophic diaphragm (Fig 2A and Supplementary Table 1). We confirmed its upregulation with real-time polymerase chain reaction (PCR) (Figure 3A). Western blotting showed a main band of osteopontin at 69 kDa in both normal and dystrophic dogs before and after the respiration (Figure 3B and 3C). The main band sizes were roughly comparable to data in other reports[11,12]. The 69 kDa osteopontin level before and after the respiration in dystrophic dogs was

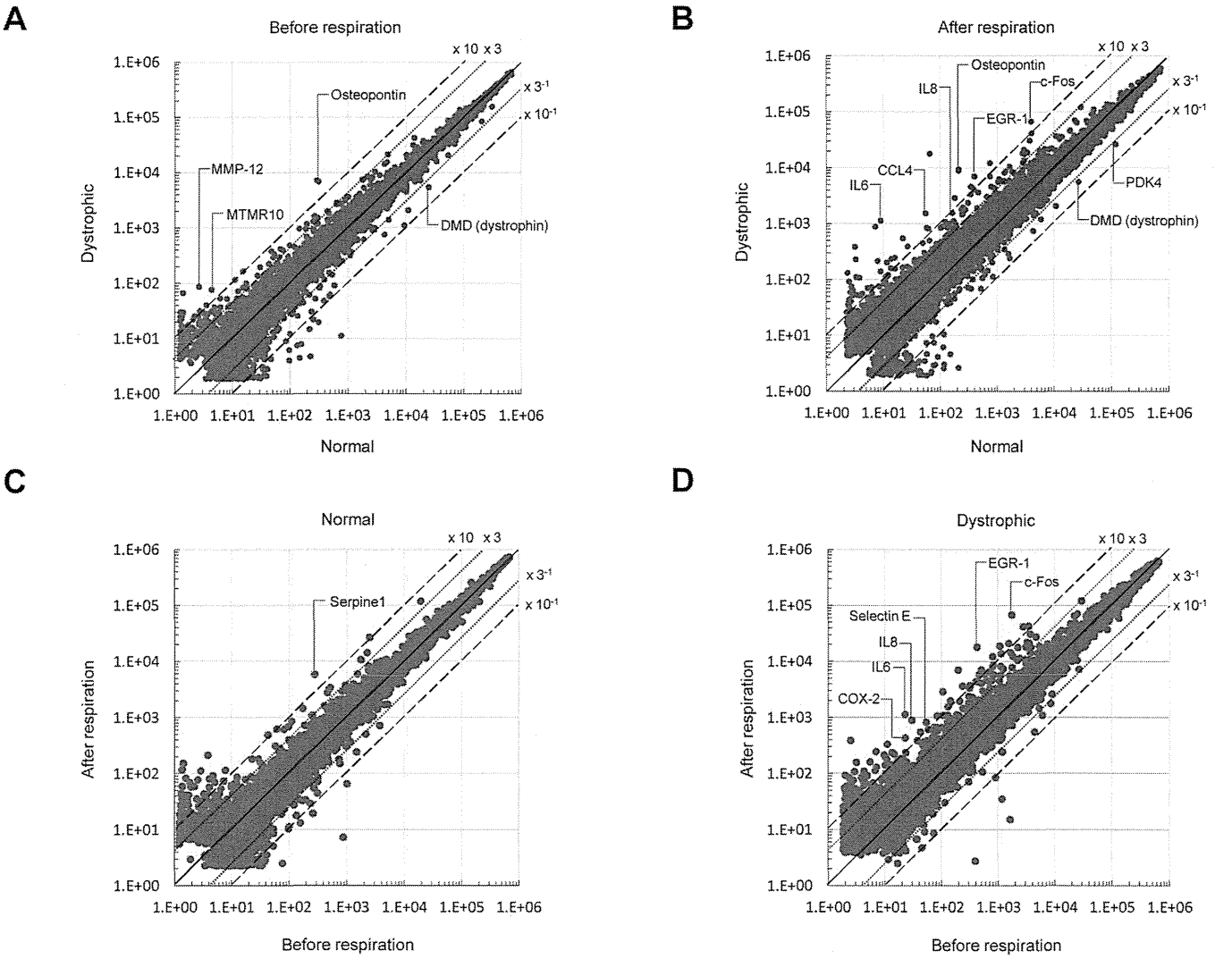

Figure 2 | Differential expressed genes in dystrophic diaphragm before and after initial respiration. (A) A scatter plot of differentially expressed genes on microarrays before respiration in normal and dystrophic diaphragms (n = 4, each). (B) A scatter plot of differentially expressed genes in normal and dystrophic diaphragms (n = 4, each) after initial respiration. (C) A scatter plot of differentially expressed genes in the normal diaphragm before and after respiration (n = 4, each) in the normal diaphragm. (D) A scatter plot of differentially expressed genes before and after respiration (n = 4, each) in the dystrophic diaphragm (cutoff: 3.0-fold).

Table 1 | Classifications of differentially upregulated (> 3-fold) genes in dystrophic to normal diaphragm, before respiration

Category	No. of genes	% of total
Transcription/signal transduction	2	4.1
Inflammation/immune response	11	22.4
Proteolysis	2	4.1
Growth	0	0
Development	0	0
Metabolism	4	8.2
Extracellular matrix	8	16.3
Membrane	14	28.6
Apoptosis	0	0
Muscle structure	1	2
Others	7	14.3
Total	49	100

Table 3 | Classifications of differentially upregulated (> 3-fold) genes after to before respiration, in normal diaphragm

Category	No. of genes	% of total
Transcription/signal transduction	12	20.3
Inflammation/immune response	6	10.2
Proteolysis	1	1.7
Growth	4	6.8
Development	5	8.5
Metabolism	3	5.1
Extracellular matrix	4	6.8
Membrane	12	20.3
Apoptosis	2	3.4
Muscle structure	0	0
Others	10	16.9
Total	59	100

significantly increased compared to that in normal dogs, although the difference was not outstanding compared to mRNA levels (Figure 3D). Immunohistochemistry revealed that osteopontin was localized in infiltrated mononuclear cells expressing CD11b, but not CD3, and the nearby muscle surfaces (Figure 3E). Moreover, overexpression of osteopontin mRNA and protein were detected not only before but also after the respiration (Figure 2B, Figure 3, and Supplementary Table 1).

Besides osteopontin, *matrix metalloproteinase-12* (*MMP-12*) mRNA level prominently upregulated in dystrophic diaphragm before the respiration (Figure 2A and Supplementary Table 1), and their upregulation were confirmed by real-time PCR (Supplementary Figure 4A). Myotuburalin related protein 10 (MTMR10) mRNA level was about 18-fold higher in dystrophic dog diaphragm compared to that of normal dog before respiration, and its level dropped rapidly to 1% of the pre-respiration level in dystrophic dog after respiration (Figure 2A and Supplementary Table 1). Real-time PCR analysis was compatible to the data of microarray (Supplementary Figure 4B).

Transcription/signal transduction and inflammation/immune response genes prominently overexpressed after diaphragm damage in neonatal dystrophic dogs. When compared the upregulated genes on microarrays between before and after the initial respiration in dystrophic diaphragm, we found that transcription/signal transduction genes (*c-fos* and *Egr-1*), and inflammatory/immune response cytokine genes (*IL6*, *IL8*, *COX-2*, and *selectin E*) were over 10-fold increased after the respiration (Figure 2D and Supplementary Table 1). Then, we examined their expression and localization of c-fos, Egr-1, IL6 and IL8. The levels of mRNA and protein of these molecules were significantly increased after the damaged dystrophic diaphragm (Figure 4A–B). c-Fos and EGR-1 localized either in the nuclei or cytoplasm of muscle fibers, and IL6 and IL8 were expressed in the muscle cytoplasm, especially in the damaged dystrophic diaphragm (Figure 4C). We also confirmed the increased mRNA levels of *COX-2* and *selectin E* in dystrophic diaphragm after the respiration using real-time PCR (Supplementary Figure 4).

Discussion

Our study demonstrated for the first time that the acute mechanical load of the initial respiration caused severe diaphragm damage in neonatal dystrophic dogs, and subsequently led to high serum CK levels and to respiratory distress. The muscle maturation in both normal and dystrophic dogs is considerably delayed compared to that in other animals and humans[13]. Respiratory overload in the immature respiratory muscles of dystrophic dogs may explain the respiratory distress following their birth. We found slight dystrophic changes in the absence of dynamic activity of dystrophic dog diaphragm prior to initial respiration. While, it was reported that fetal respiratory movements occurred before the delivery and are considered to be regular muscular contraction preparing initial respiratory movement of neonatal period[14]; therefore, the fetal respiratory movements might affect the diaphragm changes.

Before the initial respiration, the differentially upregulated genes detected by cDNA microarrays were related to inflammatory/immune response such as interleukins, cytokines or chemokines. This implies that the upregulation of these genes might affect the slight dystrophic change. Among the genes, osteopontin mRNA was mostly prominently upregulated in the dystrophic diaphragm. Osteopontin is an extracellular matrix protein with cytokine, chemokine, and cell signaling properties, can recruit neutrophils and

Table 2 | Classifications of differentially upregulated (> 3-fold) genes in dystrophic to normal diaphragm, after respiration

Category	No. of genes	% of total
Transcription/signal transduction	20	24.4
Inflammation/immune response	17	20.7
Proteolysis	4	4.9
Growth	2	2.4
Development	1	1.2
Metabolism	3	3.7
Extracellular matrix	4	4.9
Membrane	19	23.1
Apoptosis	3	3.7
Muscle structure	0	0
Others	9	11.0
Total	82	100

Table 4 | Classifications of differentially upregulated (> 3-fold) genes after to before respiration, in dystrophic diaphragm

Category	No. of genes	% of total
Transcription/signal transduction	21	24.7
Inflammation/immune response	10	11.8
Proteolysis	3	3.5
Growth	4	4.7
Development	4	4.7
Metabolism	5	5.9
Extracellular matrix	7	8.2
Membrane	14	16.5
Apoptosis	4	4.7
Muscle structure	2	2.4
Others	11	12.9
Total	85	100

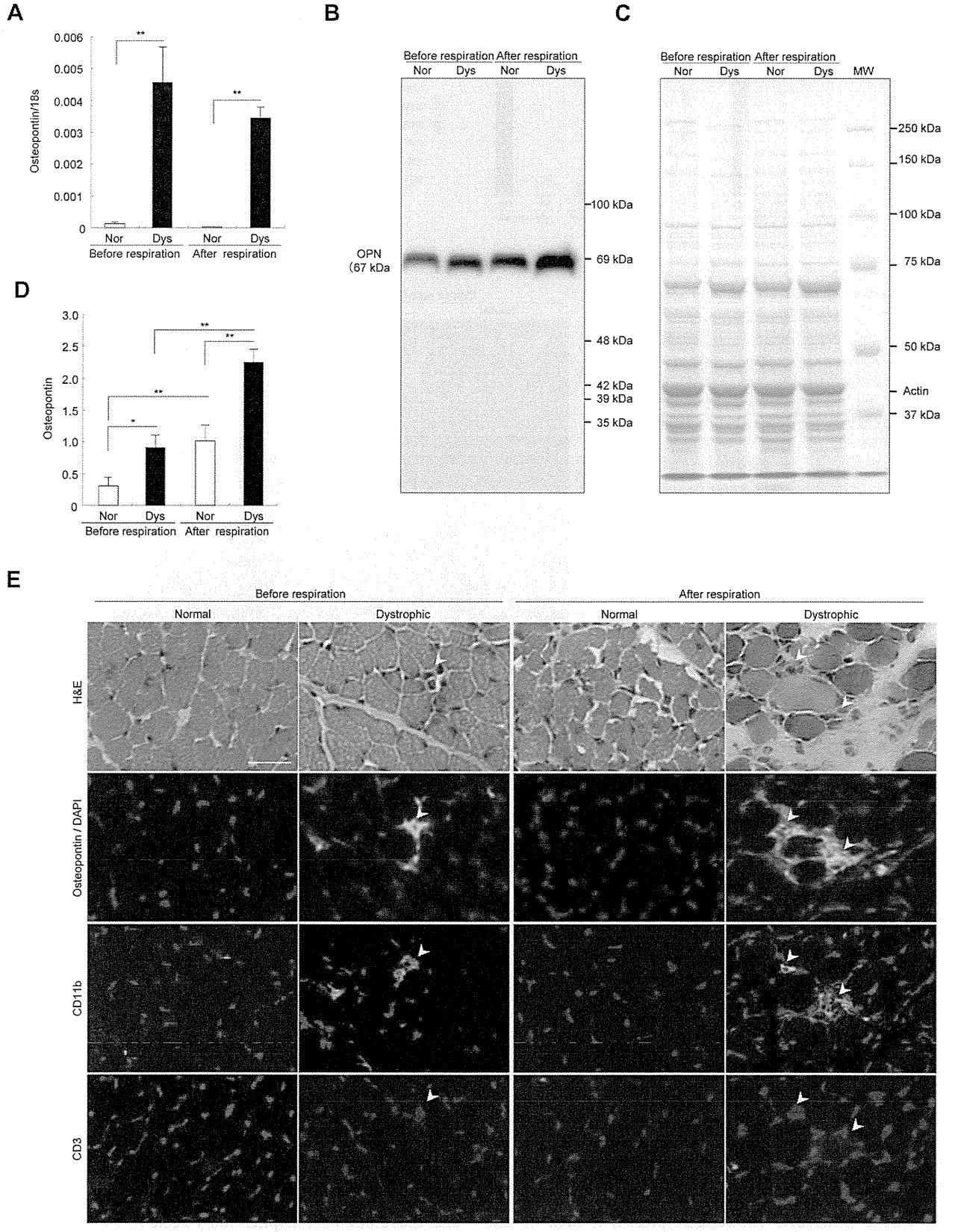

Figure 3 | Osteopontin upregulated before the diaphragm damage in neonatal dystrophic dogs. (A) Comparison of relative osteopontin mRNA levels to 18 s in normal (Nor) and dystrophic (Dys) dogs before (n = 4, each) and after (n = 4, each) the respiration. Bar: mean ± SD; ** $p < 0.01$. (B) Western blotting of osteopontin and (C) CBB staining of diaphragms in normal and dystrophic dogs before and after respiration. Actin: loading control. The short and long exposure blots are included in the supplementary information. (D) Comparison of relative levels of 69 kDa osteopontin to actin in normal (Nor) and dystrophic (Dys) dogs before (n = 4, each) and after (n = 4, each) the respiration. Bar: mean ± SD; ** $p < 0.01$. (E) Hematoxylin-eosin (H&E) staining of diaphragms of normal and dystrophic dogs before respiration and 1 hour after respiration. Immunohistochemistry of osteopontin, CD11b, CD3 (all green), and DAPI (blue) in normal and dystrophic dogs before and after respiration. Bar indicates 100 μm.

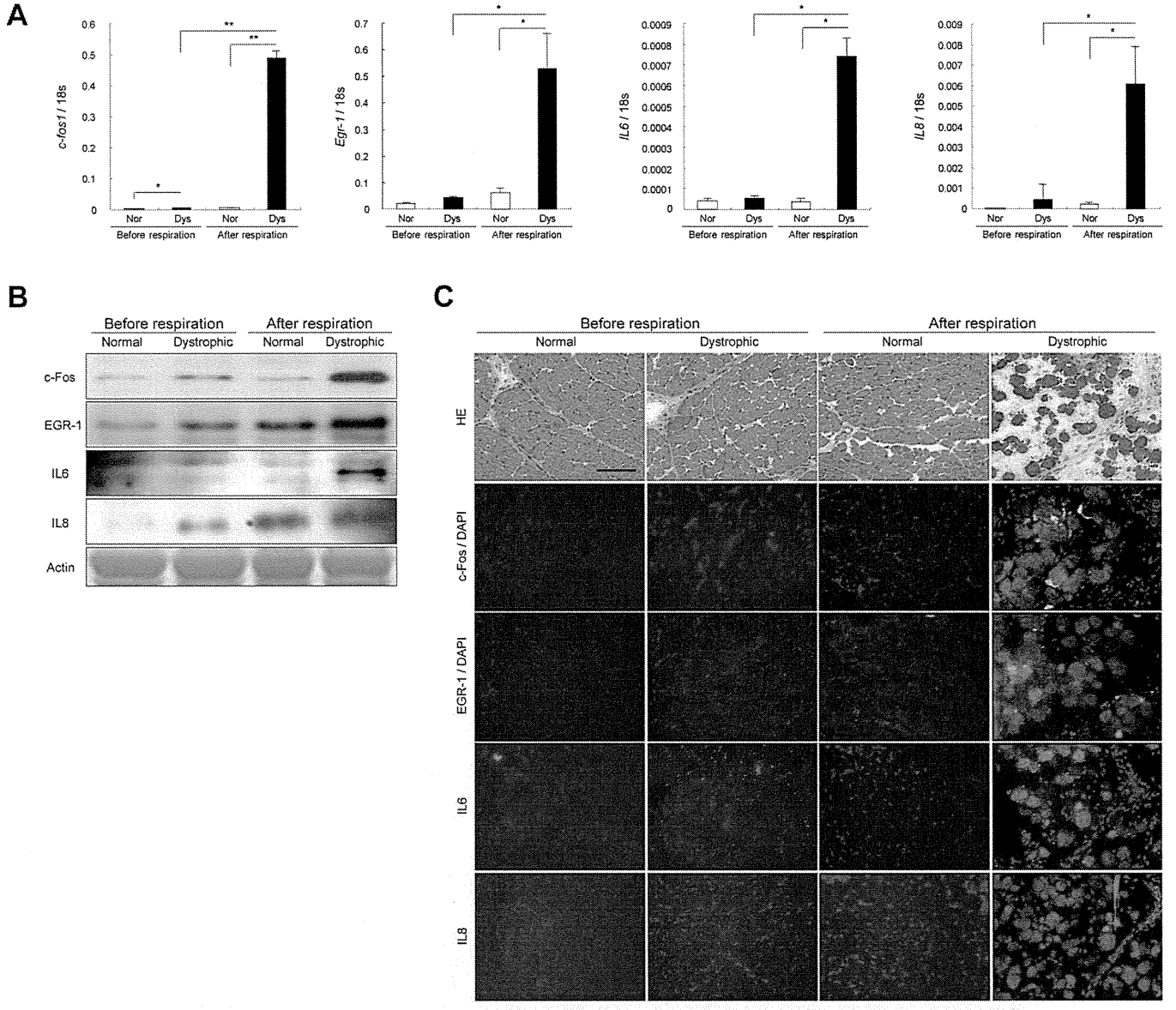

Figure 4 | *c-fos, egr-1*, IL6, and IL8 overexpressed after diaphragm damage in neonatal dystrophic dogs. (A) Comparison of relative mRNA levels of *c-fos*, *egr-1*, *IL6*, and *IL8* in normal (Nor) and dystrophic (Dys) dogs before (n = 4, each) and after (n = 4, each) the respiration. Bar: mean ± SD; * $p < 0.05$; ** $p < 0.01$; *** $p < 0.001$. (B) Western blotting of c-Fos, EGR-1, IL6, and IL8 in normal and dystrophic dogs before and after the respiration. Actin: loading control. The blots and gels are cropped and the full-length gels and blots are included in the supplementary information. (C) H&E and immunohistochemistry of c-Fos, EGR1, IL6, IL8 (all green), and DAPI (blue) in the dystrophic diaphragm before respiration. Bar indicates 100 μm.

macrophages[15]. It has already been reported that osteopontin was produced by dystrophic muscle itself and inflammatory cells such as CD68-positive macrophages or CD3-positive T-cells[16]. Our results showed that osteopontin was expressed in CD11b-positive monocytes/macrophages and nearby muscle surfaces. Here, we have raised a question why monocytes/macrophages were recruited in the dystrophic diaphragm even before the initial respiration. Our microarray analyses revealed that monocyte/macrophage recruiting chemokine CCL-2 (monocyte chemotactic protein-1: MCP-1) and CCL-4 (macrophage inhibitory protein-1β: MIP-1β), which are designated as muscle-produced cytokines (myokines)[17,18], were significantly upregulated even before the initial respiration (Supplementary Table 1). Indeed, osteopontin has been reported to be induced by CCL-2 and CCL-4 in synovial fluid of rheumatoid arthritis[19]. Thus, we have proposed that these myokines may recruit monocytes/macrophages and subsequently lead to induction of osteopontin.

In the role of osteopontin in dystrophic muscle, it has been proposed that osteopontin mediates the early phase of muscle regeneration in injured muscle[20] or promotes fibrosis in dystrophic muscle[21]. Recently, it has been reported that osteopontin stimulates expression of MMP-9 resulting in causing cardiomyopathy in the *mdx* mice[22]. We and other researchers have previously reported that MMP-9 can be associated with the dystrophic muscle degeneration[23,24]. Indeed, MMP-9 was upregulated (4.1-fold) dystrophic diaphragms especially after the respiration (Supplementary Table 1). Taken all, osteopontin may induce muscle degeneration in dystrophic diaphragms, and have an essential role from the very early to the late stages of dystrophic pathology. Currently, osteopontin is considered to be a potential target for therapeutic intervention in DMD[21,25]. We found the distinct upregulation of MMP-12 in the dystrophic diaphragms after the respiration. A recent paper showed that cleavage of osteopontin by MMP-12 modulates experimental autoimmune encephalomyelitis in C57BL/6 mice[26]. In our result, the cleavage pattern of

osteopontin was slightly different between normal and dystrophic diaphragms. Thus, MMP-12 might affect osteopontin processing in dystrophic diaphragm, and further studies will be needed to examine the relationship between the molecules.

Myotuburalin related protein 10 (MTMR10) mRNA level was also distinctly higher in dystrophic dog diaphragm before respiration compared to that of normal dog. MTMR10 is one of MTMRs, which comprise a large family of ubiquitously expressed lipid phosphatases[27]. Among MTMRs, MTMR2 has recently been linked to neurodegenerative disorder Charcot-Marie-Tooth disease type 4B and myotubralin (MTM1) is mutated in a muscle disorder X-linked myotubular myopathy[27]. Although the role and function of MTMR10 and its related disorder have not been identified, this molecule might have a certain role in the dystrophic pathology and we would leave it as a future study.

In damaged dystrophic diaphragms after the respiration, *c-fos*, *egr-1*, IL6, and IL8 were prominently upregulated. The upregulation of *c-fos*, *egr-1*, and IL8 in dystrophic diaphragms has not been observed prior to this study. Moreover, the overexpression of IL6 has not evoked much attention since Kurek *et al.* reported an increase in IL6 expression in dystrophic muscle[28]. *c-fos* and *egr-1* are immediate-early genes that are regulated by a local increase in Ca^{2+} concentration[29,30] and induce a number of downstream genes, including IL6[31] and IL8[32]. Both IL6 and IL8 are myokines and upregulated in exercised normal skeletal muscle[17]. IL6 may maintain metabolic homeostasis in normal muscle[33], but as a pro-inflammatory cytokine, IL6 may play a role in dystrophic pathology resulting from damage by mechanical load. IL8 is a major chemokine that recruits neutrophils after injurious mechanical strain[34]. Indeed, our results showed that a neutrophil recruitment related gene *selectin E*[35] was strongly upregulated in dystrophic diaphragm after the respiration. It has been reported that neutrophil accumulation in muscle is evident within 2−6 h after muscle injury[34]. Thus, we have examined the muscle pathology 2.5 hours after the initial respiration in dystrophic diaphragm. Infiltration of CD-18 positive neutrophil was observed in the damaged dystrophic muscle (Supplementary Figure 5). A previous report indicated that neutrophils play a central role in the initial dystrophic pathology since antibody depletion of host neutrophils significantly reduces muscle necrosis[36]. COX-2 was also distinctly upregulated in dystrophic diaphragm after the respiration compared to before. In general, COX-2 is lower expressed in every tissue except for brain and kidney; however, is highly induced in inflammatory tissues. COX-2 leads to the production of prostaglandins resulted in the progression of inflammation by promotion of vascular permeability and vasodilatation[37]. Recently, it has been reported that anti-inflammatory drugs inhibiting COX-2 could reduce necrosis in *mdx* mouse[38,39]. Thus, we hypothesize that the dystrophic process after mechanical load consists initially of sarcolemmal disruption and afterward, some major genes and molecules such as *c-fos*, *egr-1*, IL6, IL8, selectin E, and COX-2 promote sterile inflammation in the dystrophic muscle, resulting in the aftermath of a necrotic event.

In this study, we have for the first time revealed the molecular mechanism of very early stage of damage in dystrophin-deficient muscle as a result of mechanical load. The mechanism presented here could also occur in the skeletal muscle of human DMD patients. However, degeneration and regeneration concurrently operate in the tissues of these patients[40], so that the molecular mechanism associated with each pathology cannot be identified[41]. By studying the neonatal dystrophic dog diaphragm, we succeeded at segregating the dystrophic phases into those before and after mechanical injury. In the treatment of DMD, the promising therapeutic agent corticosteroid improves muscle function[42], but the underlying mechanism of its action is not fully understood. Corticosteroids strongly reduce the production of IL6, IL8[43], and COX-2[44]; therefore, the genes and molecules reported here may not only be biomarkers of muscle damage but also molecular targets in pharmaceutical therapies to prevent disease progression.

Methods

Experimental dogs. For comparisons of serum CK levels and mortality rates, we used normal (n = 71), carrier (n = 37), and dystrophic (n = 41) pups obtained by 39 natural deliveries, and normal (n = 39), carriers (n = 26), and dystrophic (n = 34) pups derived from 28 Caesarean sections between December 2001 and April 2008. The dogs were born in the dystrophic dog ($CXMD_J$) breeding colony at the General Animal Research Facility, National Institute of Neuroscience, National Center of Neurology and Psychiatry (NCNP) (Tokyo, Japan). Elective Caesarean sections were performed at the expected delivery date based on the results of an LH surge kit (Witness® LH, Synbiotics, Kansas City, MO, USA) or when the body temperature of the pregnant carrier dog decreased acutely. Pregnant dogs were induced and maintained by inhalation of isoflurane (2.0–3.0%) for general anesthesia, and pups were surgically delivered by Caesarean sections. After the sections, placental membranes should be removed from the neonate's body and head, and the umbilical cord should be clamped and ligated approximately 2 cm from the body. The oropharynx should be cleared of respiratory secretions and swinging the neonate to remove secretions is widely practiced. The chest wall should be vigorously rubbed not only to remove placental fluids but also to stimulate spontaneous breathing. Vocalization is a good sign that the lungs are well expanded. Supplemental oxygen should be provided by face mask or by placing the puppies in an oxygen induction chamber once spontaneous respiration. Puppies should be immediately dried with a warm, dry towel and placed under a radiant heat source. We routinely used doxapram in neonates delivered by Caesarean sections to stimulate spontaneous respiration because it is extensively used in veterinary neonatal respiration[45]. For the histopathological and molecular analyses, we have obtained all samples after the euthanasia but not naturally died after birth.

To determine the time course of serum CK values, we used normal (n = 5), carrier (n = 3), and dystrophic (n = 6) dogs derived from three additional Caesarean sections. We performed the histopathological and molecular biological experiments on dogs (n = 4) in each group delivered in the Caesarean sections mentioned above. The experiments were conducted under the guidelines provided by the Ethics Committee for the Treatment of Laboratory Animals of the National Institute of Neuroscience (Tokyo, Japan), and were approved by the Ethics Committee for the Treatment of Laboratory Middle-Sized Animals of the National Institute of Neuroscience (approval Nos. 13-03, 14-03, 15-03, 16-03, 17-03, 18-03, 19-04, and 20-04). We performed experiments with consideration for preventing excessive pain.

Determination of serum creatine kinase (CK) level. The blood samples from the umbilical cord at Caesarean sections and the jugular vein of each dog were taken using a syringe, and the serum was separated by centrifugation at 1,800 *g* for 10 min at room temperature. Among the dogs, we measured serum CK levels in cord blood of normal (n = 5), carrier (n = 3), and dystrophic (n = 6) dogs at 30 min, 1, 2, 4, 8, 24, and 48 h. Serum CK levels were assayed using an automated colorimetric analyzer (FDC3500, FujiFilm Medical, Tokyo, Japan).

Histopathology and immnunohistochemistry. After euthanasia, diaphragm, tibialis cranialis (TC) and heart (left ventricle) muscles were snap-frozen in cooled isopentane. Cryostat sections 7 μm thick were cut and stained with hematoxylin and eosin (H&E) or alizarin red, pH 4.1, for 20 min at room temperature to visualize the cytosolic calcium. Some sections were dried for 15 min and pre-incubated with phosphate-buffered saline (PBS) containing 5% bovine serum albumin or heat-inactivated normal goat serum albumin at pH 7.4. The sections were incubated with primary antibodies for 16 hrs at 4°C, then with fluorescein isothiocyanate (FITC)-labeled secondary antibodies (10 μg/ml) at room temperature for 1 h before washing in 5% BSA. The sections were mounted using Fluorescent Mounting Medium with DAPI (Vector Laboratories, Burlingame, CA, USA) and assessed under fluorescence microscopes BZ-9000 (Keyence, Osaka, Japan) and Eclipse E600 (Nikon, Tokyo, Japan). Primary antibodies used were: CD3 (C7930, Sigma-Ardrich, St Louis, MO, USA), CD11b (MCA1777S, AbD Serotec, Oxford, UK), CD18 (MCA1780, AbD Serotec), C5b-9 (ab66768, Abcam, Cambridge, UK), cleaved caspase 3 (#9661, Cell Signaling Technology, Beverly, MA, USA), LC3 (#4108, Cell Signaling Technology), osteopontin (RB-9097, Thermo Fisher Scientific, Waltham, MA, USA), c-Fos (#2250, Cell Signaling Technology), EGR-1 (#4153, Cell Signaling Technology), IL6 (sc-80108, Santa Cruz Biotechnology, Santa Cruz, CA, USA), and IL8 (109-401-311, Rockland Immunohistochemical, Gilbertsville, PA, USA).

Western blotting. Diaphragm muscles were homogenized in sample buffer (62.5 mM Tris-HCl, pH 6.8, 2% sodium dodecyle sulfate, 10% glycerol), or T-PER Tissue Extraction Reagent for osteopontin (Thermo Fisher Scientific, Waltham, MA, USA). After centrifugation (15,000 *g* for 10 min), the supernatant was removed and the protein concentration was assayed using a DC Assay kit (BioRad, Hercules, CA, USA). Protein homogenates were denatured at 95°C for 5 min or 70°C for 10 min for osteopontin. Ten or forty micrograms of each muscle extract was separated on 5-15% XV Pantera Gel (DRC, Tokyo, Japan) or 7% NuPAGE Tris-Acetate Gel (Life Technologies, Carlsbad, CA, USA) for osteopontin, and either transferred to a polyvinylidene difluoride membrane or stained with Coomassie Brilliant Blue (CBB). The membranes were blocked in Tris-buffered or phosphate-buffered saline containing 0.1% Tween 20 (TBST or PBST) and 2% or 5% skim milk (w/v), and then incubated with a primary antibody to osteopontin (RB-9097, Thermo Fisher Scientific), c-Fos (#2250, Cell Signaling Technology), EGR-1 (sc-189, Santa Cruz Biotechnology), IL6 (AF1609, R&D Systems, Minneapolis, MN, USA), or IL8 (ab34100, Abcam, Cambridge, UK) at 4°C overnight. The membranes were washed in

TBST and then incubated with a mouse- or rabbit-specific horseradish peroxidase-conjugated secondary antibody, followed by detection using an enhanced chemiluminescence ECL-Plus Western Blotting Detection System (GE HealthCare, Buckinghamshire, UK).

cDNA microarray. Diaphragm muscles from normal and dystrophic dogs before and after initial respiration (n = 4, each) were snap-frozen in liquid nitrogen and stored at −80°C. Total RNA was purified using an RNeasy Mini Kit (Qiagen, Hilden, Germany) according to the manufacturer's protocols. The RNA concentration was also determined using a NanoDrop® ND-1000 UV-Vis spectrophotometer (NanoDrop Technologies, Wilmington, DE, USA). RNA quality was checked using an Agilent Bioanalyzer 2100 (Agilent Technologies, Santa Clara, CA, USA). Total RNA (500 ng) was extracted from normal and dystrophic dogs, and individually applied to a whole canine genome oligo microarray 44 K (Agilent Technologies). Hybridization was performed by Bio Matrix Research Co., Ltd. (Nagareyama, Chiba, Japan). Briefly, 500 ng of RNA was converted to double-stranded cDNA with an RNA SpikeIn kit (one color) (Agilent Technologies) using a T7 promoter primer, followed by transcription to generate Cy3-labelled cRNA probes with Quick Amp Labeling Kit (Agilent Technologies). Fragmented cRNA (1.65 μg) was placed in 110 μl hybridization solvent, and then placed on each chip, which was incubated at 65°C for 17 hrs rotating at 60 rpm. Following hybridization, the arrays were processed by post-hybridization washes. Fluorescent images were captured using an Agilent Technologies microarray scanner (Agilent Technologies). Global normalization was performed to compare genes from chip to chip using GeneSpring 10.0 (Tomy Digital Biology, Denver, CO, USA). Differentially expressed genes were identified by comparison between normal and dystrophic dogs before and after respiration. The differentially expressed genes were selected by ANOVA tests. $P < 0.01$ with correction for multiple testing by the Benjamini and Hochberg method for the false discovery rate, and a 5% cutoff was used. The array data were deposited in the Gene Expression Omnibus (GEO) database (Accession number: GSE32460).

Relative gene expression based on real-time RT-PCR. We picked up the genes from the microarray analyses by using of the cutoff of value as 10-fold. We used the same RNA that was isolated for the DNA microarrays and prepared cDNA using SuperScript III Reverse Transcriptase (Invitrogen, Carlsbad, CA, USA). Gene-specific primer sets for the previously published dog 18 s rRNA and newly designed *osteopontin, c-fos, egr-1, IL6, IL8, COX-2, Selectin E, MMP-12, and MTMR10* mRNA are listed in Supplemental Table 2. The primer specificity was tested by running a regular PCR for 40 cycles of 95°C for 20 s and 60°C for 1 min, followed by agarose gel electrophoresis. The mRNA levels were analyzed by real-time quantitative RT-PCR using a Bio-Rad iCycler system (Bio-Rad) and a SYBR premix Ex Taq II kit (Takara, Tokyo, Japan), and running for 40 cycles of 95°C for 20 s and 60°C for 1 min. Each cDNA sample was duplicated, and the corresponding no-RT mRNA sample was included as a negative control. The mRNA level of each sample for each gene was normalized to that of the 18 s rRNA. The relative mRNA level was presented as $2\,[(C_t/18\text{ s rRNA} - C_t/\text{gene of interest})]$. Expression values were normalized to 18 s rRNA and compared between normal and dystrophic dogs before and after the initial respiration in (n = 4, each).

Statistics. Direct comparisons between 2 groups of data were performed using the Student's unpaired *t*-test. Multiple statistical differences between groups were compared by one-way analysis of variance (ANOVA) followed by Holm's post-hoc test. All data are indicated as mean values ± standard error of the mean (SEM). A $p < 0.05$ was judged to be a significant difference.

1. Sarkis, J. *et al.* Resisting sarcolemmal rupture: dystrophin repeats increase membrane-actin stiffness. *FASEB* **27**, 359–369 (2012).
2. Jørgensen, L. H. *et al.* Long-term blocking of calcium channels in mdx mice results in differential effects on heart and skeletal muscle. *Am J Pathol* **178**, 273–83 (2011).
3. Tanabe, Y., Esaki, K. & Nomura, T. Skeletal muscle pathology in X-chromosome-linked muscular dystrophy (mdx) mouse. *Acta Neuropathol (Berl.)* **69**, 91–95 (1986).
4. Valentine, B. A., Cooper, B. J., de lahunta, A., O'Quinn, R. & Blue, J. T. An animal model of Duchenne muscular dystrophy: clinical studies. *J Neurol Sci* **88**, 69–81 (1988).
5. Shimatsu, Y. *et al.* Major clinical and histopathological characteristics of canine X-linked muscular dystrophy in Japan, CXMDJ. *Acta Myologica* **24**, 145–154 (2005).
6. Heyck, H., Laudahn, G. & Carsten, P. M. Enzymatktivitätsbestimmungen bei dystrophia musculorum progressia. IV. Mitterilung. Die serumenzymkinetik im präklinischen stadium des typus Duchenne während der ersten 2 lebensjahre. *Klin Wochnschr* **44**, 695–700 (1966).
7. Demos, J. Early diagnosis and treatment of rapidly developing Duchenne de Boulogne type myopathy (type DDBI). *Am J Phys Med* **50**, 271–284 (1971).
8. Zellweger, H. & Antonik, A. Newborn screening for Duchenne muscular dystrophy. *Pediatrics* **55**, 30–34 (1975).
9. Rudolph, N. & Gross, R. T. Creatine phsophokinase activity in serum of newborn infants as indicator of fetal trauma during birth. *Pediatrics* **38**, 1039–1046 (1966).
10. Drumond, L. M. Creatine phosphokinase levels in the newborn and their use in screening for Duchenne muscular dystrophy. *Arch Dis Child* **54**, 362–366 (1979).
11. Agnihotri, R. *et al.* Osteopontin, a novel substrate for matrix metalloproteinase-3 (stromelysin-1) and matrix metalloproteinase-7 (matrilysin). *J Biol Chem* **276**, 28261–28267 (2001).
12. Goncalves DaSilva, A., Liaw, L. & Yong, V. W. Cleavage of osteopontin by matrix metalloproteinase-12 modulates experimental autoimmune encephalomyelitis disease in C57BL/6 mice. *Am J Pathol* **177**, 1448–1458 (2010).
13. Lanfossi, M. *et al.* Development of muscle pathology in canine X-linked muscular dystrophy. I. Delayed postnatal maturation of affected and normal muscle as revealed by myosin isoform analysis and utrophin expression. *Acta Neuropathol* **97**, 127–138 (1999).
14. Malney, J. E., Alcom, D., Bowes, G. & Wilkinson, M. Development of the future respiratory system before birthe. *Semin Perinatol* **4**, 251–260 (1980).
15. Scatena, M., Liaw, L. & Giachelli, C. M. Osteopontin: a multifunctional molecule regulating chronic inflammation and vascular disease. *Arterioscler Thromb Vasc Biol* **27**, 2302–2309 (2007).
16. Zanotti, S. *et al.* Osteopontin is highly expressed in severely dystrophic muscle and seems to play a role in muscle regeneration and fibrosis. *Histopathology* **59**, 1215–1228 (2011).
17. Pedersen, B. K., Åkerström, T. C., Nielsen, A. R. & Fischer, C. P. Role of myokines in exercise and metabolism. *J Appl Physiol* **103**, 1093–1098 (2007).
18. Mathers, J. A., Farnfield, M. M., Garnham, A. P., Caldow, M. K. & Cameron-Smith, D. Early inflammatory and myogenic responses to resistance exercise in the elderly. *Muscle Nerve* **46**, 407–412 (2012)
19. Zheng, W. *et al.* Role of osteopontin in induction of monocyte chemoattractant proein 1 and macrophage inflammatory protein 1beta through the NF-kappaB and MAPK pathways inrheumatoid arthritis. *Arthritis Rheum* **60**, 1957–1965 (2009)
20. Hirata, H. *et al.* Expression profiling of cytokines and related genes in regenerating skeletal muscle after cardiotoxin injection: a role for osteopontin. *Am J Pathol* **163**, 203–205 (2003).
21. Vetrone, S. A. *et al.* Osteopontin promotes fibrosis in dystrophic mouse muscle by modulating immune cell subsets and intramuscular TGF-beta. *J Clin Invest* **119**, 1583–1594 (2009).
22. Dahiya, S. *et al.* Osteopontin-stimulated expression of matrix metalloproteinase-9 causes cardiomyopathy in the mdx model of Duchenne musucular dystrophy. *J Immnol* **187**, 2723–2731 (2011).
23. Fukushima, K. *et al.* Activation and localization of matrix metalloproteinase-2 and -9 in the skeletal muscle of muscular dystrophy dog ($CXMD_J$). *BMC Musculoskelet Disord* **8**, 54 (2007).
24. Dahiya, S. *et al.* Elevated levels of active matrix metalloproteinase-p cause hypertrophy in skeletal muscle of normal and dystrophin-deficient mdx mice. *Hum Mol Genet* **20**, 4345–4359 (2011).
25. Qureshi, M. M. *et al.* The dietary supplement protandium decreases plasma osteopontin and improves markers of oxidative stress in muscular dystrophy mdx mice. *J Diet Suppl* **7**, 159–178 (2010).
26. DaSilva, A. G., Liaw, L. & Yong, V. W. Cleavage of osteopontin by matrix metalloproteinase-12 modulates experimental autoimmune encephalomyeltitis disease in C57BL/6 mice. *Am J Pathol* **177**, 1448–1458 (2010).
27. Wishart, M. J. & Dixon, J. E. PTEN and myotubularin phosphatases: from 3-phosphoinositide dephosphorylation to disease. *TRENDS in Cell Biol* **12**, 579–585 (2002).
28. Kurek, J. B., Nouri, S., Kannourakis, G., Murphy, M. & Austin, L. Leukemia inhibitory factor and interleukin-6 are produced by diseased and regenerating skeletal muscle. *Muscle Nerve* **19**, 1291–1301 (1996).
29. Schaefer, A., Magocsi, M., Fandrich, A. & Marquardt, H. Stimulation of the Ca2+-mediated egr-1 and c-fos expression in murine erythroleukaemia cells by cyclosporin A. *Biochem J* **355**, 505–511 (1988).
30. Grembowicz, K. P., Sprague, D. & McNeil, P. L. Temporary disruption of the plasma membrane is required for c-fos expression in response to mechanical stress. *Mol Biol Cell* **10**, 1247–1257 (1999).
31. Schuringa, J. J., Timmer, H., Luttickhuizen, D., Vellenga, E. & Kruijer, W. c-Jun and c-Fos cooperate with STAT3 in IL-6-induced transactivation of the IL-6 respone element (IRE). *Cytokine* **14**, 78–87 (2001).
32. Cullen, E. M., Brazil, J. C. & O'Connor, C. M. Mature human neutrophils constitutively express the transcription factor EGR-1. *Mol Immunol* **47**, 1701–1709 (2010).
33. Febbraio, M. A. & Pedersen, B. K. Muscle-derived interleukin-6: mechanisms for activation and possible biological roles. *FASEB J* **16**, 1335–1347 (2002).
34. Peterson, J. M. & Pizza, F. X. Cytokines derived from cultured skeletal muscle cells after mechanical strain promote neutrophil chemotaxis in vitro. *J Appl Physiol* **106**, 130–137 (2009).
35. McDonald, B. & Kubes, P. Cellular and molecular choreography of neutrophil recruitment to site of sterile inflammation. *J Mol Med* **89**, 1079–1088 (2011).
36. Hodgetts, S., Radley, H., Davies, M. & Grounds, M. D. Reduced necrosis of dystrophic muscle by depletion of host neutrophils, or blocking TNFalpha function with Etanercept in mdx mice. *Neuromuscl Disord* **16**, 591–602 (2006).
37. Gilroy, D. W. & Volville-Nash, P. R. New insights into the role of COX-2 in inflammation. *J Mol Med* **78**, 121–129 (2000).
38. Messina, S. *et al.* Flavocoxid counteracts muscle necrosis and improves functional properties in mdx mice: a comparison study with methylprednisolone. *Exp Neurol* **220**, 349–358 (2009).

39. Serra, F. *et al.* Inflammation in muscular dystrophy and the beneficial effects of non-steroidal anti-inflammatory drugs. *Muscle Nerve* **46**, 773–784 (2012).
40. Uchino, M., Araki, S. & Miike, T. Correlative study of the incidence of opaque, necrotic and regenerative fibers in Duchenne dystrophy. *Acta Neuropathol* **75**, 308–312 (1988).
41. Noguchi, S. *et al.* cDNA microarray analysis of individual Duchenne muscular dystrophy patients. *Hum Mol Genet* **12**, 595–600 (2003).
42. Bushby, K. *et al.* Diagnosis and management of Duchenne muscular dystrophy, part 1: diagnosis, and pharmacological and psychosocial management. *Lancet Neurol* **9**, 77–93 (2010).
43. Frieri, M. Corticosteriod effects on cytokines and chemokines. *Allergy Asthma Proc* **20**, 147–159 (1999).
44. Malcher-Lopes, R., Franco, A. & Tasker, J. G. Glucocorticoids shift arachidonic acid metabolism toward endocannabinoid synthesis: a non-genomic anti-inflammatory switch. *Eur J Pharm* **583**, 322–339 (2008).
45. Kobayashi, M. *et al.* Evaluation of dystrophic dog pathology by fat-suppressed T2-weighted imaging. *Muscle Nerve* **40**, 815–826 (2009).

Acknowledgements

We thank Hideki Kita, Shin'ichi Ichikawa, Yumiko Yahata, Takayuki Nakayama, Kazue Kinoshita, Ryoko Nakagawa, Yuko Kasahara, Takashi Saito, and Michihiro Imamura (Department of Molecular Therapy) for their technical assistance. This work was supported by a Grant-in-Aid for Research on Nervous and Mental Disorders (19A-7), a Health Sciences Research Grant for Research on Psychiatric and Neurological Diseases and Mental Health (H18-kokoro-019), a Health and Labor Sciences Research Grants for Translational Research (H19-Translational Research-003 and H21-Clinical Research-015) from the Ministry of Health, Labor and Welfare of Japan, and a Grants-in-Aid for Scientific Research (B) from The Ministry of Education, Culture, Sports, Science and Technology of Japan (21300157 to AN).

Author contributions

A.N. conducted the experiments and wrote the manuscript; M.K., M.K. and N.Y. performed the experiments and Caesarean sections on our colony dogs; K.Y., T.O. and S.T. participated in data interpretation and supervised the study, execution, and manuscript preparation. All authors reviewed the manuscript.

Additional information

Supplementary information accompanies this paper at http://www.nature.com/scientificreports

Competing financial interests: The authors declare no competing financial interests.

How to cite this article: Nakamura, A. *et al.* Initial Pulmonary Respiration Causes Massive Diaphragm Damage and Hyper-CKemia in Duchenne Muscular Dystrophy Dog. *Sci. Rep.* **3**, 2183; DOI:10.1038/srep02183 (2013).